A MORPHOLOGICAL APPROACH TO THE AUTOMATIC DETECTION OF DARK FRINGES APPLIED TO BIREFRINGENCE IMAGES

Lucas A. Thomaz†, Allan F. da Silva†, Eduardo A. B. da Silva†, Sergio L. Netto†
André M. Castro‡, Juliana O. Pereira‡, Argimiro R. Secchi‡
{lucas.thomaz,allan.freitas,eduardo,sergioln}@smt.ufjr.br
†PEE–‡PEQ, COPPE, Universidade Federal do Rio de Janeiro, Brazil

ABSTRACT

This work presents a novel approach to detect automatically the position of dark fringes in birefringence images. These positions are important for rheology (study of the flow of matter) applications, as they allow indirect measurements of physical properties of molten polymers without having to interact with the material. Our approach uses mathematical morphology techniques to find the patterns that characterize the fringes and detect the center position of each one of them. The results are compared with manual measurements, revealing the superior precision of our method. They have also been applied to the calculation of the stress field of some polymers with good results.

Index Terms— Morphological Operations , Birefringence, Watershed, Fringe Detection

1. INTRODUCTION

The study of the flow properties of a fluid has many applications in industrial processes. In order to improve the industrial efficiency and avoid trial-and-error procedures, the relations between the rheological properties of a polymer and its physical characteristics must be studied [1–3].

A rheo-optical technique to analyze physical properties of polymers that has recently resurfaced is the flow induced birefringence [4]. This approach is based on inducing a birefringence property on a fluid due to orientation of the polymer chains during flow and infering the stress levels in the flowing polymer melts by relating it to the birefringence using the stress-optical rule(SOR) [5–9]. This rule states that the resulting image light pattern provides information about the spatial evolution of the stress in the molten polymer. This technique is successfully employed in [10] to distinguish between two polystyrene grids and assess specific characteristics during a complex industrial process.

One of the characteristics that must be analyzed when dealing with birefringence images is the position of black fringes. The manual measurement of these positions is quite time consuming and prone to errors. The aim of this paper is to propose a method, based on mathematical morphology, that allows such measurements to be performed automatically, yielding faster and more precise results.

In birefrigence experiments [11], the patterns of bright and dark fringes are converted to a stress profile along the fluid flow. Along the centerline, the shear stress component is zero and the principal stress difference (PSD) is equal to the first normal stress difference, and after some development [10]:

$$\text{PSD} = |\text{N}_1| = \frac{k\lambda}{|C|\,d}, \tag{1}$$

Thanks to CNPq for funding

where $k = 1, 2, ..., n$ is the fringe order (see Fig. 1), λ is the monochromatic polarized-light wavelenght, d is the depth of sample through which the light propagares and C is the stress-optical coefficient that relates the stress and the index of refraction.

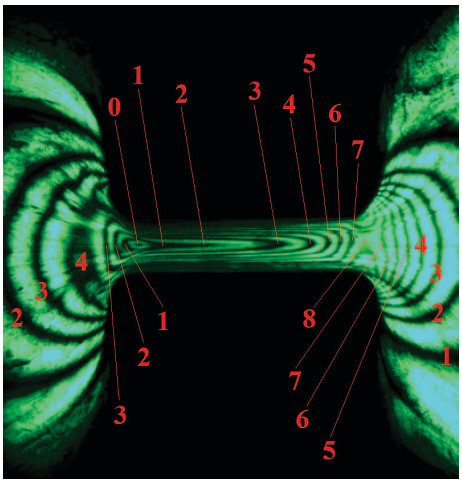

Fig. 1. Classical arrangements for birefringence observations showing the fringe order, whose centers are to be detected. (Adapted from [10])

Equation 1 shows that having the position of each black fringe and knowing the values of parameters given by the experiment, one can determine the first normal stress difference along the centerline of the outflow.

In order to introduce the proposed algorithm, the remaining of this paper is organized as follows: Section 2 presents the most efficient fringe detection techniques in the literature. A step-by-step description of the proposed fringe position detector is given in Section 3. Section 4 shows experimental results illustrating the capabilities of the proposed system and the conclusions are presented in Section 5.

2. FRINGE DETECTION TECHNIQUES

There are several approaches to perform computer-aided fringe detection on interference fields. Methods based on image binarization [12] generate a mask to separate the bright and dark fringes. This mask is then used to create a centerline for each fringe by applying morphological procedures like thinning or skeletonisation. Some techniques find local intensity maxima and minima and track the intensity distribution [13]. Other methods employ differential

filters [14].

The most widely employed techniques on fringe detection model the periodic characteristics of the fringes as a carrier modulated by a signal [15]. Fourier techniques are used to obtain characteristics such as the fringe position along the centerline [16]. These techniques are improved by the phase shifting algorithm [17, 18], which uses a series of phase shifted interferograms to estimate fractional fringe orders. Random phase-shifting algorithms [19, 20] provide further improvements.

The proposed method deals with images recorded on a very noisy framework, presenting variations in the dynamic range over time. These preclude the use of intensity and binarization-based techniques. Also, since such images can present several discontinuities and interferences between fringes, approaches based on the fringe periodicity should also be avoided.

The approach used to deal with such noisy images is to employ morphological techniques — such as watershed and top-hat/bottom-hat operations — to simplify their structure, enabling a reliable determination of the position of the black-fringe centers. This information is then employed on the estimation of a pressure profile of the polymer used on the experiment.

3. FRINGE POSITION DETECTION

The proposed method for detecting the positions of the black-fringe centers is implemented in 4 steps, as illustrated in Fig. 2. In the following subsections, implementation details are provided for these 4 algorithm stages.

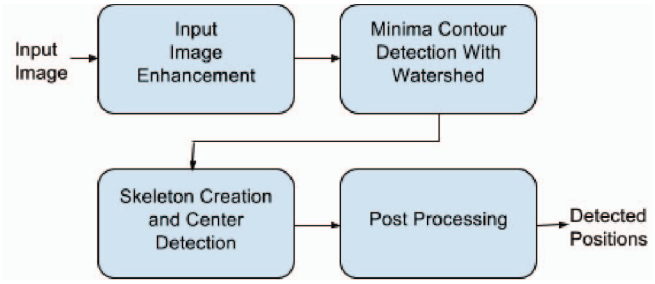

Fig. 2. Block diagram of the proposed method.

3.1. Input image enhancement

In the intended application, the input images are usually ill conditioned, since the distinction of the light and dark fringes can be hard to make. Some usual problems related to this issue are: gaps in the clear fringes that unduly connect dark fringes, and "leakages" in the light fringes making the dark ones fade between two consecutive bright ones. Most of these problems are related to the noise present in the experiment, creating poorly contrasted input images.

The approach chosen to deal with this issue is to add to the input image its morphological top-hat [21] and subtract its bottom-hat [21]. The result is an image whose maxima and minima are better defined.

Some examples of these problems and the results after the top-hat/bottom-hat processing can be seen in Fig. 3.

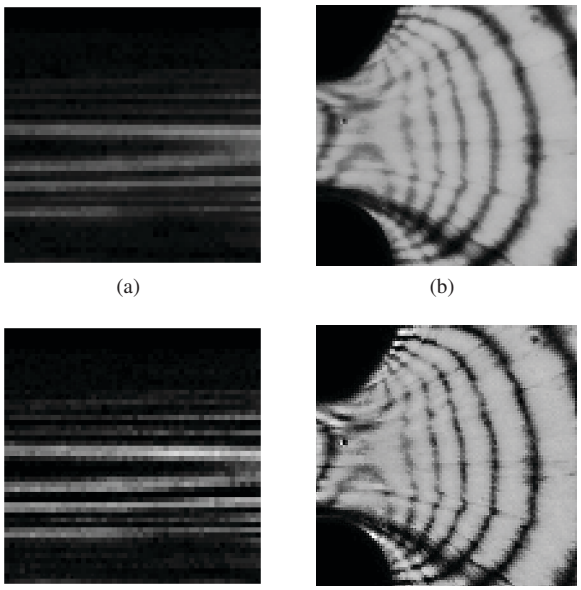

Fig. 3. Image enhancement using top-hat and bottom-hat techniques. (a) and (b): original images; (c) and (d): enhanced images.

3.2. Minima contour detection with watershed

The rationale behind the proposed method is to relate the centers of black fringes to the contours associated with the minima of the enhanced image. However, as one can see from the images in Fig. 3, these minima are ill defined. We solve this problem by associating these minima to the contours obtained with the watershed transformation [22] applied to the complement of the enhanced image. The initial results related to the application of the watershed method to the image are shown in Fig. 4(a). One can see that, as is common in such cases, there is a lot of oversegmentation on the image, yielding unreliable results for the center estimation of the black fringes. We dealt with this problem by introducing an initial minimum imposition step [23] prior to the watershed transformation. Note that the initial minima position should be provided by a human operator, by indicating any point inside each light fringe. Fig. 4(b) illustrates that indeed the initial minima imposition was effective in alleviating the oversegmentation issue. Note that, although the minima imposition step is manual, it only needs to be performed in the first image of the birefringence set, as illustrated in Section 3.4. Therefore, the method can be considered automatic for all but the first image (it is common to process a sequence of 50 birefringence images).

3.3. Skeleton creation and center detection

The watershed transformation often generates contours that are connected by spurious branches (see Fig. 4(b)), which can be removed by enforcing contours that are only one pixel wide. To perform this step a skeletonisation technique [24] is used. Here the original contours are replaced by the locus of the center of the maximal discs of the original contour lines.

We define the distance between fringes as the distance between their minima contours at the center of the birefringence image. Thus, after the skeletonisation process we process only a region-of-interest composed by a horizontal stripe at the centerline of the contour im-

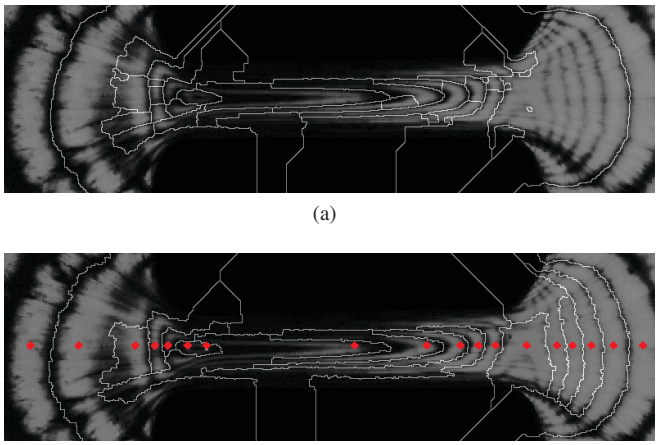

(a) (b)

Fig. 4. Minima contours detected with watershed. (a) Whitout minima imposition — the image is oversegmented and some dark fringes are undetected. (b) With minima imposition — the oversegmentation issue is alleviated and the contours are better detected.

age.

The next step is the removal of the branching points of the region-of-interest. One considers branching points the ones that are connected to three or more points. After this step, the contour image is composed of several segments of connected pixels. Then, those segments whose number of connected pixels is smaller than a pre-set threshold are eliminated, leaving only the relevant segments to the image. An example of the result of this processing step is shown in Fig. 5.

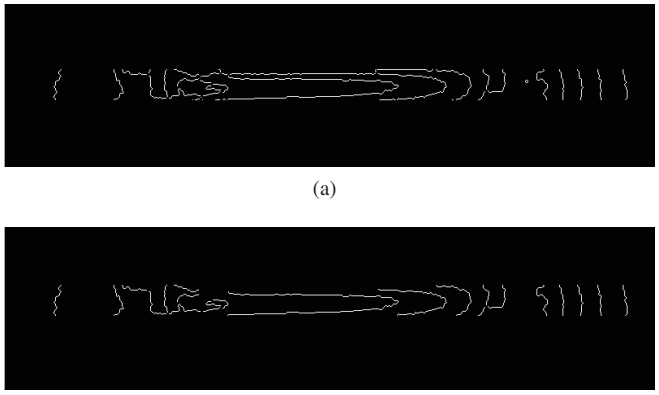

(a) (b)

Fig. 5. Elimination of spurious points and short segments: (a) Connected points before processing. (b) Connected points after the removal of spurious points.

Once the relevant segments are selected, one needs to find the distance between them. In order to do so we assume that the distance will be measured between the contour points that constitute approximately local maxima or local minima in height (see Fig. 6(b)). We do so with the help of a small horizontal window. The part of the segment that contains the larger number of points inside the window is considered to be the desired one. Fig. 6 illustrates that process.

After the application of the sliding window a few segments that

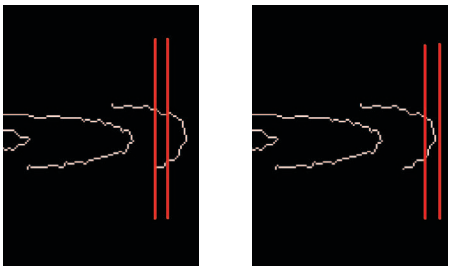

(a) (b)

Fig. 6. Selection of points representing the center of the dark fringes. (a) Wrong selection — fewer segment points. (b) Right selection — most segment points.

do not represent the required minima contour of the dark fringes can still remain. These spurious segments can be eliminated by another selection step. Since between each pair of consecutive imposed minima there is only one visible dark fringe, the algorithm keeps the largest segment inside the region confined by those points. For each of those remaining segments, the center position of the corresponding dark fringe is selected as the average horizontal position of all points inside the window.

3.4. Post-processing

After the detection of the center of dark fringes it is necessary to perform one further detection. Referring to Fig. 1 the fringe labeled as 8 must be identified although not visible; it is in fact a saddle point. To perform this detection, the positions of the bright regions surrounded by black 'C'-shaped fringes were included as minima to be imposed. After performing the watershed step, the 'C'-shaped dark regions must also have a minima contour. A similar procedure to that employed in the dark-fringe center detection is used to identify the middle point of the 'C'-shaped lines, by using a horizontal window instead of a vertical one and disregarding any minima contour in the center of the image. The saddle point is estimated as the average of the middle positions, as illustrated in Fig. 7.

Fig. 7. Detection of the saddle point (marked as a red spot) based on the dark fringes.

Whenever an object composed by contour minima cannot be found in the fringe region, the output warns the user to allow a manual correction step on those fringes. However, the algorithm also provides an estimate based purely on the minima imposition input provided, by averaging the surrounding bright points, so the algorithm always provides an estimate on the fringe positions for the user to judge whether they are correct or if they must placed manually.

The algorithm can also perform a temporal interpolation on the missing points. When measuring several images from a time-

evolving experiment, some fringes can be missing in a given time but appear in another image sample. Since those positions should not vary widely over time, by the end of the experiment any missing position is interpolated by the closest frames where this fringe could be found. A similar procedure is carried out for the imposed minima - only the first frame of a sequence has to have a manual minima imposition - the ones from the other frames are estimated by temporal extrapolation.

4. EXPERIMENTAL RESULTS

The described algorithm was developed in a MATLAB© [25] environment using morphological function implementations present on the Image Processing Toolbox. The technique was tested in 54 images acquired using LabVIEW© [26] from a flow experiment with a multi-pass rheometer. The software requires that an operator inputs a few minima to be imposed in the first frame, which are used in all subsequent images from the same experiment.

Some results of the fringe-center detection can be seen in Fig. 8. The white vertical lines mark the position of each fringe center. The blue vertical line marks the position of the detected saddle point. If a dark fringe center could not be detected, the algorithm estimates its position based on the minima points imposed by the operator and draws it as a red vertical line, as discussed above.

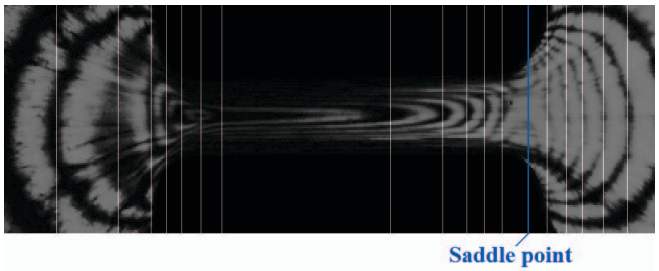

(a)

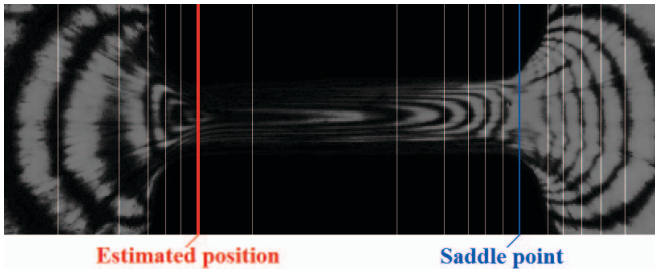

(b)

Fig. 8. Results of the algorithm for two birefringence images. The white lines represent the detected fringe positions, the blue line represents the saddle point and the red line is the estimated position when a fringe center could not be found.

After applying the procedure to the entire dataset (composed by 54 birefringence images), the dark-fringe positions of the whole process were estimated, along with its second order moment. This result is compared to a manual marking of the same points, as shown in Tab. 1. From this table it is possible to see that both approaches have almost the same mean but the proposed method has smaller standard deviations, which shows better consistency.

Table 1. Comparison of the algorithm results and the manual marking for the fringe positions (in pixel), indexed accordingly to Fig. 1.

Fringe	Algorithm Results		Manual Marking	
Order	Mean	Variance	Mean	Variance
3	66.83	4.33	63.24	31.51
4	136.78	36.31	133.37	11.03
3	180.67	5.36	178.76	1.92
2	198.83	3.05	197.29	0.63
1	216.51	16.05	216.15	0.58
0	241.01	25.03	238.76	0.68
2	281.39	1328.39	307.30	32.17
3	474.67	76.60	475.00	1726.38
4	537.50	13.46	536.00	169.40
5	568.77	5.52	563.44	1673.76
6	591.43	7.49	591.02	17.00
7	613.39	52.42	610.81	15.25
8	641.05	119.33	639.22	20.74
7	666.30	24.41	666.69	42.14
6	689.17	8.14	689.54	9.91
5	710.16	3.73	710.80	2.62
4	734.11	3.61	734.63	2.58
3	765.44	2.97	765.94	3.56

The final results allow the modeling of the principal stress difference along the centerlines of the polymer flow by the use of Eq. 1. Fig. 9 presents the principal stress difference for the positions acquired from the algorithm and the manual marking, showing great similarity between the results obtained by both schemes.

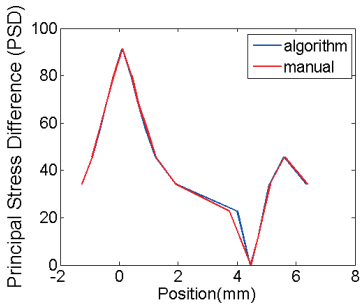

Fig. 9. Principal Stress Difference as a function of distance along centerline.

5. CONCLUSIONS

This work presents a novel approach to the problem of detecting dark fringes in birefringence images. The proposed method allows fast and accurate measurement of the dark-fringe centers while minimizing the need of human interaction with the images. The described algorithm can operate with minimum human intervention.

An evaluation of the results has been made to compare the obtained results with a database of marked fringes available online at [27]. The results have shown to be consistent with those of manual marking, while having significantly less variance.

When applied to the calculation of indirect physical properties of the polymers using noisy birefringence images, our results have accurately mimicked the expected curves, confirming the good behavior of the method in real practical situations.

6. REFERENCES

[1] R. B. Bird, R. C. Armstrong, and O. Hassager, *Dynamics of Polymeric Liquids*, John Wiley & Sons, New York, 1st edition, 1987.

[2] C. W. Macosko, *Rheology: principles, measurements and applications*, Wiley-VCH, New York, 1994.

[3] R. G. Larson, *Constitutive equations for polymer melts and solutions*, Butterwork Publishers, Boston, 1988.

[4] G. C. Berry, "Optical rheometry of complex fluids," *Journal of Solution Chemistry*, vol. 25, no. 9, pp. 919–920, September 1996.

[5] A. S. Lodge, "Variation of flow birefrigence with stress," *Nature*, vol. 176, pp. 838–839, October 1955.

[6] L. M. Quinzani, R. C. Armstrong, and R. A. Brown, "Birefringence and laser-doppler velocimetry (ldv) studies of viscoelastic flow through a planar contraction," *Journal of Non-Newtonian Fluid Mechanics*, vol. 52, no. 1, pp. 1–36, April 1994.

[7] R. Ahmed, R. Liang, and M. Mackley, "The experimental observation and numerical prediction of planar entry flow and die swell for molten polyethylenes," *Journal of Non-Newtonian Fluid Mechanics*, vol. 59, no. 2-3, pp. 129–153, September 1995.

[8] K. Lee and M. Mackley, "The application of the multi-pass rheometer for precise rheo-optic characterisation of polyethylene melts," *Chemical Engineering Science*, vol. 56, no. 19, pp. 5653–5661, 2001.

[9] M. Collis and M. Mackley, "The melt processing of monodisperse and polydisperse polystyrene melts within a slit entry and exit flow," *Journal of Non-Newtonian Fluid Mechanics*, vol. 128, no. 1, pp. 29–41, June 2005.

[10] T. M. Farias, A. R. Secchi, S. Butler, and N. S. M. Cardozo, "Utilização da técnica de birrefringência em reômetro multipasse para a diferenciação de grades de poliestireno cristal," *Polímeros*, vol. 24, pp. 596–603, October 2014.

[11] R. Muller and B. Vergnes, *Rheology for Polymer Melt Processing*, Elsevier, 1996.

[12] M. Farooq, A. Aslam, B. Hussain, G. Hussain, and M. Ikram, "A comparison of image processing techniques for optical interference fringe analysis," *Photonic Sensors*, vol. 5, no. 4, pp. 304–311, 2015.

[13] G. Ye and L. Wei, "A method for interference fringe fast skeletonizing," in *2012 2nd International Conference on Computer Science and Network Technology (ICCSNT)*, December 2012, pp. 1784–1786.

[14] Q. Yu and K. Andresen, "Fringe-orientation maps and fringe skeleton extraction by the two-dimensional derivative-sign binary-fringe method," *Applied Optics*, vol. 33, no. 29, pp. 6873–6878, October 1994.

[15] M. EL-Morsy, "A new algorithm for automatic double bright fringe of multiple-beam fizeau fringe skeletonization using fourier transform method of fringe pattern analysis," *Journal of Signal and Information Processing*, vol. 3, no. 3, pp. 412–419, 2012.

[16] T. Z. N. Sokkar, H. M. El Dessouky, M. A. Shams-Eldin, and M. A. El-Morsy, "Automatic fringe analysis of two-beam interference patterns for measurement of refractive index and birefringence profiles of fibres," *Optics and Lasers in Engineering*, vol. 45, no. 3, pp. 431–441, 2007.

[17] C. Y. Poon, M. Kujawinska, and C. Ruiz, "Automated fringe pattern analysis for moiré interferometry," *Experimental Mechanics*, vol. 33, no. 3, pp. 234–241, September 1993.

[18] J. M. Huntley, "Automated fringe pattern analysis in experimental mechanics: A review," *The Journal of Strain Analysis for Engineering Design*, vol. 33, no. 2, pp. 105–125, January 1998.

[19] Z. Wang and F. Dai, "Automatic fringe patterns analysis using digital processing techniques II: phase analysis method," *Acta Photonica Sinica*, vol. 28, pp. 996–1001, 1999.

[20] Wang Z. and Han B., "Enhanced random phase shifting technique," in *2004 SEM X International Congress & Exposition on Experimental & Applied Mechanics*, Costa Mesa, California, 2004.

[21] F. Meyer, "Iterative image transformations for an automatic screening of cervical smears," *The Journal of Histochemistry and Cytochemistry*, vol. 27, no. 1, pp. 128–135, January 1979.

[22] S. Beucher and C. Lantuéj, "Use of watersheds in contour detection," in *International workshop on image processing, real-time edge and motion detection*, September 1979.

[23] P. Soille, *Morphological Image Analysis: Principles and Applications*, Springer-Verlag, Secaucus, NJ, USA, 2nd edition, 2003.

[24] C. Arcelli and C. Sanniti di Baja, "Euclidean skeleton via centre-of-maximal-disc extraction," *Image and Vision Computing*, vol. 11, no. 3, pp. 163–173, April 1993.

[25] MATLAB, *version 8.0.0.783 (R2012b)*, The MathWorks Inc., Natick, Massachusetts, 2012.

[26] LABVIEW, *version 15.0f2*, National Instruments Corp., Austin, Texas, 2015.

[27] "Birrefringence experiment data," `http://www2.peq.coppe.ufrj.br/Pessoal/Professores/Arge/MPR/`, Accessed 2016-01-22.